Anatomically based finite element models of the human pulmonary arterial and venous trees including supernumerary vessels

Kelly S. Burrowes, Peter J. Hunter and Merryn H. Tawhai

J Appl Physiol 99:731-738, 2005. First published 31 March 2005;
doi: 10.1152/japplphysiol.01033.2004

J Appl Physiol 99: 731–738, 2005.
First published March 31, 2005; doi:10.1152/japplphysiol.01033.2004.

Anatomically based finite element models of the human pulmonary arterial and venous trees including supernumerary vessels

Kelly S. Burrowes, Peter J. Hunter, and Merryn H. Tawhai
Bioengineering Institute, The University of Auckland, Auckland, New Zealand

Submitted 24 September 2004; accepted in final form 29 March 2005

Burrowes, Kelly S., Peter J. Hunter, and Merryn H. Tawhai. Anatomically based finite element models of the human pulmonary arterial and venous trees including supernumerary vessels. *J Appl Physiol* 99: 731–738, 2005. First published March 31, 2005; doi:10.1152/japplphysiol.01033.2004.—Studies of the origin of pulmonary blood flow heterogeneity have highlighted the significant role of vessel branching structure on flow distribution. To enable more detailed investigation of structure-function relationships in the pulmonary circulation, an anatomically based finite element model of the arterial and venous networks has been developed to more accurately reflect the geometry found in vivo. Geometric models of the arterial and venous tree structures are created using a combination of multidetector row X-ray computed tomography imaging to define around 2,500 vessels from each tree, a volume-filling branching algorithm to generate the remaining accompanying conducting vessels, and an empirically based algorithm to generate the supernumerary vessel geometry. The explicit generation of supernumerary vessels is a unique feature of the computational model. Analysis of branching properties and geometric parameters demonstrates close correlation between the model geometry and anatomical measures of human pulmonary blood vessels. A total of 12 Strahler orders for the arterial system and 10 Strahler orders for the venous system are generated, down to the equivalent level of the terminal bronchioles in the bronchial tree. A simple Poiseuille flow solution, assuming rigid vessels, is obtained within the arterial geometry of the left lung, demonstrating a large amount of heterogeneity in the flow distribution, especially with inclusion of supernumerary vessels. This model has been constructed to accurately represent available morphometric data derived from the complex asymmetric branching structure of the human pulmonary vasculature in a form that will be suitable for application in functional simulations.

pulmonary vasculature; computational modeling; pulmonary imaging

EXPERIMENTAL STUDIES TO INVESTIGATE the origin of pulmonary blood flow heterogeneity (7, 8, 11) have suggested that nongravitational mechanisms play a far greater role than was suggested by earlier studies (34). Normal variations in lung tissue material properties, the branching vascular tree, regional gas volumes, and the position of the heart are just a few of the interacting components influencing blood flow distribution in the lung. The contribution of the structure of the pulmonary vascular tree to blood flow heterogeneity has previously been investigated using computational models (3, 9, 19, 24).

Previous evaluations of the structure-function relationship in the pulmonary circulation via mathematical techniques have reduced the complexity of the pulmonary vascular tree geometry by, for example, representing the pulmonary arteries and veins as a symmetric tree (24), or as a self-similar fractal tree (1, 9, 19), or by representing an average flow path via summary morphometric parameters (3). These models have been implemented to investigate the effects of large-scale alterations of branching geometry on hemodynamics in the lung and, therefore, only represent the average geometry of the branching structure. The models have not been created to accurately reflect the geometry of the vascular structure; they have instead been designed for use in a particular functional investigation. These studies all illustrate the large dependence of flow distribution on network geometry. While these simplified models represent the complicated structure with a small number of parameters and provide useful insights into the relationship between structure and function, they do neglect several features known or predicted to be present.

Although these previous models have been based on anatomical measures, they cannot represent the geometry of an individual subject, nor do they provide accurate spatial information. This limits their application in computational studies in which the vessel's three-dimensional (3D) orientation is important, for example, if correlations between imaging data and model results need to be made. "Anatomically based" models, such as presented by Tawhai et al. (31) for the human bronchial airways, and developed further by Tawhai et al. (29) for the human and ovine airway tree, are derived from medical imaging and have subject-specific 3D branching geometry. This type of model accurately represents the measured average geometry of the airway tree and has a further advantage of relating individual airways to their location in the lung. The vascular models created in this study are of the same nature, whereby the future possibilities of coupling structural or functional imaging information to computational modeling will allow specific structure-function relationships to be investigated.

Each bronchial airway is accompanied by an arterial vessel, but there are many more pulmonary arterial vessels than there are branches in the bronchial tree; the same is true for the venous system. These vessels, which do not have a corresponding bronchial airway, have been termed "supernumerary" blood vessels, and they occur throughout the length of the pulmonary vascular system, from the hilum to the level of the capillaries, but have been found to be more numerous toward the lung periphery (5). These very small vessels tend to bud at right angles from the accompanying blood vessels and branch rapidly to directly supply the closest pulmonary acinus. Through a combination of measurement and extrapolation, the ratio of supernumerary to accompanying terminal arteries has been estimated at ~2.8:1; the ratio for the venous supernumerary vessels is estimated to be even higher, at ~3.5:1 (4).

Address for reprint requests and other correspondence: K. S. Burrowes, Bioengineering Institute, The Univ. of Auckland, Private Bag 92019, Auckland, New Zealand (E-mail: k.burrowes@auckland.ac.nz).

The costs of publication of this article were defrayed in part by the payment of page charges. The article must therefore be hereby marked "*advertisement*" in accordance with 18 U.S.C. Section 1734 solely to indicate this fact.

Previous models of the pulmonary vascular trees have not explicitly differentiated the supernumerary vessels from the accompanying vessels, yet these vessels have unique structural and functional differences that may prove to be particularly important in computational studies that investigate perfusion heterogeneity in the normal lung, during exercise, or when a vessel is occluded.

In the current study, geometric models of the pulmonary arterial and venous trees are constructed using a combination of multidetector row computed tomography (MDCT) to identify the largest vessels, a volume-filling branching (VFB) algorithm (31) to generate the vessels that accompany airways to the level of the respiratory bronchioles, and a vessel-specific algorithm that incorporates the supernumerary arteries and veins. The focus of this study is on creating a representative geometric model for future use in several possible functional investigations. This study develops the framework for creating patient-specific models derived from MDCT scans.

METHODS

Anatomical geometry from MDCT. Gray-scale bitmap masks segmented from MDCT data of a normal, unsedated human man in the supine posture, with lungs inflated to (and held at) 90% vital capacity (7.05 liters) were obtained from the Department of Physiological Imaging at the University of Iowa. Human studies were approved by the University of Iowa Institute Review Board and Radiation Safety Committees. The masks are a resource from the Lung Atlas (20) and are the same data set used in derivation of models of the conducting airways by Tawhai et al. (29). A pitch of 1.5, collimation of 1.2, 100 mA, 120 kV, slice thickness of 1.3 mm, slice increment of 0.65 mm, reconstruction matrix size of 512 × 512, and a field of view of ~35 cm were used for the spiral scanning in a Marconi MX8000 MDCT scanner. Vessel bifurcation points and one-dimensional (1D) lines supplying connectivity information were also extracted from the Lung Atlas data. Details on the skeletonization techniques can be found in Ref. 23.

Use of a contrast agent allowed automatic identification of numerous vessels in both the arterial and venous trees (see Fig. 4*A*), but the vessels were not automatically differentiated as venous or arterial vessels. This differentiation was performed manually by first identifying the largest pulmonary arteries and veins and then following the connectivity of each tree while tagging each successive vessel as either a vein or an artery. In many locations, the arterial and venous trees passed so closely to each other that the skeletonization software (23) was unable to identify them as separate trees. In this case, the tree connectivity revealed many more than three vessels converging at a bifurcation point. In most cases, the correct classification of the vessels was clear from their orientation or from the relationship between the vessels in the next generation, but, for locations where it was not clear, no further classification of vessels was made beyond that point.

Each vessel segment (the portion of vessel between two branch divisions) was modeled as a 1D linear finite element through the center of the vessel. A finite element node was placed at each bifurcation point (at the intersection of 1D centerlines) in the segmented (and classified) tree, and the tree connectivity was described by joining elements at the appropriate nodes.

Accompanying vessels. Anatomical studies have identified a characteristic relationship between the airway, venous, and arterial trees: each airway is "accompanied" by an artery (5, 22, 32) and is more loosely followed by veins that bifurcate between neighboring airway bifurcations (33), as illustrated in the schematic diagram in Fig. 1. The branching geometry of the accompanying vessels is, therefore, very similar to the branching geometry of the airway tree. The VFB algorithm, previously used to model the airway tree (29, 31), was, therefore, used in the present study to generate accompanying arterial and venous vessels such that the models are continuous with the MDCT-derived model trees described in the previous section.

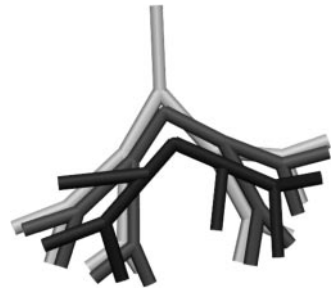

Fig. 1. Schematic diagram illustrating the relationship between the 3 conducting trees: the arteries (dark gray) closely follow the airways (light gray) with venous vessel (black) bifurcation points being positioned halfway between arterial or airway bifurcation points.

Finite element volume meshes of each of the five lobes (Fig. 2*B*) were fitted to data point clouds, generated via gray-scale information provided by lung surface masks (also obtained from the Lung Atlas) (Fig. 2*A*), using a geometry fitting procedure (6). Initial linear elements were fitted to the cloud of data points by minimizing the distance between each data point and the projection of the data point onto the element surface. Each lobe was filled with a grid of uniformly spaced seed points that were subdivided according to which MDCT-based vessel they were closest to (N MDCT-model terminal vessels = N sets of seed points). Each set of points was further divided by the plane that contained the center of mass of the points and the MDCT-model parent branch ($2N$ sets of seed points). The first VFB vessels were generated starting at the end of the corresponding MDCT-model vessel, directed toward the center of mass of the subset of points and terminating 40% of the distance to the center of mass (29, 31). This generated $2N$ new model vessels. The point reassignment (to closest terminal branch), plane splitting, and branch generation steps were repeated until either the generated length was less than a minimum length, or else the new branch supplied only a single seed point. For paths that terminated by length limit, all but the closest seed point to the end of the generated branch were reassigned to the global set of seed points for further branch generation. The VFB algorithm is described in more detail in Tawhai et al. (29).

Arterial and venous trees were generated by using the same seed point density [30,000 terminal bronchioles/7.05 liters (10)], branching fraction (distance to center of mass = 40%), and angle limit (180°) as used by Tawhai et al. (29) for modeling the conducting airway tree. Minimum vessel lengths of 1.4 and 1.8 mm were used for the arterial and venous trees, respectively. These values were chosen using the criteria that the mean length of the generated terminal branches was consistent with anatomical measurements of 1.38 mm (arteries) and 1.34 mm (veins) for the lowest order accompanying vessels (Strahler *order 7*) (13, 15).

Diameters for the MDCT-based and VFB-based trees were allocated using anatomically based Strahler diameter ratios (R_d) (13, 15), such that:

$$\log D(x) = (x - N) \log R_d + \log D_N \qquad (1)$$

where D is the computed diameter for any vessel of order x, x is the Strahler order, N is the highest vessel order, and D_N is the diameter of the vessel of highest order. Values of R_d = 1.6 (13) and 1.7 (15) were used for the arterial and venous trees, respectively.

Supernumerary vessels. An algorithm was developed to mimic the limited known geometric characteristics of supernumerary vessels and to produce models of the full venous and arterial trees with anatom-

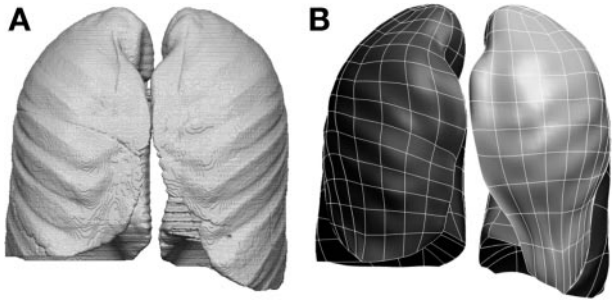

Fig. 2. Finite element model of each of the 5 lobes (shown in different grayscale colors). *A*: rendered volumetric image reconstruction from the Lung Atlas. *B*: finite element surface model obtained using a geometry fitting procedure.

ically consistent geometry. The following criteria or anatomical information was used.

Weibel (32) estimated that supernumerary branches begin to emerge when the main tract vessel has a diameter of <1.5 mm (beyond approximately the eighth generation). Supernumerary vessels were, therefore, added to branches of *generation 8* and higher in the MDCT- and VFB-based models.

Supernumerary vessels emerge at roughly 90° from the accompanying branch and branch rapidly to supply the closest parenchymal tissue.

The final tree was required to have branching ratio (R_b) close to 3.0 and 3.3 for the arterial and venous trees, respectively.

The following steps were used to generate the supernumerary vessels; this procedure is represented schematically in Fig. 3.

The mean ratio of supernumerary vessels to accompanying vessels is specified. For each vessel, the number of local supernumerary branches is calculated as the integer value ± 1 (i.e., if the overall ratio is 2.7, there will be a 70% chance of having 3 supernumerary vessels per accompanying vessel, and a 30% chance of having 2 supernumeraries per accompanying vessel). Values of 2.5:1 (arterial) and 3.0:1 (venous) were used to produce appropriate R_b.

The starting point of each supernumerary vessel is located at an evenly spaced position along the length of the accompanying vessel (i.e., if there is one supernumerary vessel, it is located halfway along the accompanying vessel), and the closest adjacent seed point from the VFB model generation (representing a single acinus) is calculated. The angle that this point makes to the parent vessel is checked to ensure that it is close to 90°; if not, the next closest point is found.

A new branch is created from the accompanying branch toward the closest acinus/seed point. The diameter of the vessel is defined as a fraction of the parent branch diameter (0.3 in the current model for both the arterial and venous systems). The length of the vessel is calculated by using length ratio (R_l) to R_d of 6:1 for the arteries (13) and 8:1 for the veins (15).

The diameter-based Strahler order of each new vessel is determined based on typical diameter ranges from anatomical data (13, 15). If it is not a terminal branch (Strahler *order 6* for the present model), the algorithm proceeds to *step 5*.

If the vessel is to bifurcate, the order number is decreased by 1, and the two closest data points are found (limited by an angle specification of between 20 and 160°), and each branch then extends toward its closest data point (which is different for each daughter). The diameter is allocated as the average anatomical diameter value for the new Strahler order number of the vessel; the length is set as specified in *step 3*. The supernumerary vessel successively bifurcates in this manner until a terminal order vessel is obtained, or until the vessel reaches a VFB seed point.

Analysis of branching geometry. Each full model tree (MDCT based, accompanying, and supernumerary vessels) was classified by Strahler order. The R_b, R_d, and R_l were calculated for each of MDCT vessels only, MDCT plus accompanying vessels, and MDCT plus accompanying plus supernumerary vessels. Branching angles were calculated for the complete model, where θ_{branch} is the angle between a parent and a child branch, and γ (rotation angle) is the angle between the plane containing the parent branch and its sibling and the plane containing the two daughter branches. The angles between the parent and the major (θ_{major}) and minor (θ_{minor}) child branches were also calculated, where the minor branch is classified as the branch with the smallest diameter, or, if both daughter branch diameters are equal, the minor branch is defined as the branch with the largest branch angle; the major branch is the other branch of the two.

Simple flow solution within the arterial model geometry. A simple Poiseuille flow solution (*Eq. 2*), assuming rigid vessels and laminar flow and incorporating conservation of mass at each junction, is obtained within the arterial vascular geometry of the left lung. Although studies have estimated that the Reynolds number (=diameter × velocity/kinematic viscosity) may exceed 2,000 (the approximate upper limit for laminar flow) in the largest pulmonary arterial vessels, turbulent flow probably does not occur and certainly does not occur in smaller vessels, where the Reynolds number is much lower (16).

$$R = \frac{\Delta P}{Q} = \frac{128 \mu L}{\pi D^4} \quad (2)$$

where R, ΔP, and Q are the resistance, pressure drop, and flow within a vessel, respectively. The viscosity of blood (μ) has an assumed value of 0.003 Pa/s, and L and D are the length and diameter of the vessel, respectively. A solution can be obtained by specifying pressure boundary conditions at the pulmonary trunk inlet (pressure = 2 kPa) and at all terminal arterial locations (pressure = 1.25 kPa). Comparison is made between the flow solution in the arterial model geometry of the left lung with and without supernumerary vessels. The Poiseuille flow solution is also obtained within a symmetric arterial model (within the left lung), with approximately the same number of

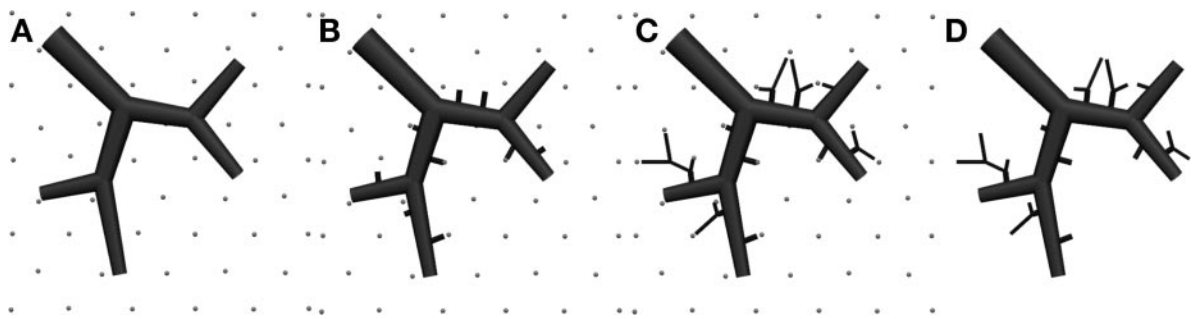

Fig. 3. Schematic illustration of the supernumerary algorithm. *A*: starting with the accompanying blood vessels and a uniformly distributed grid of points within the lung volume (each point representing an acinar unit). *B*: supernumerary branches emerge at right angles from the accompanying branch and grow toward the closest point. *C* and *D*: vessels branch and continue to grow toward the closest point, until the point is reached or an *order 6* (terminal order) vessel is obtained.

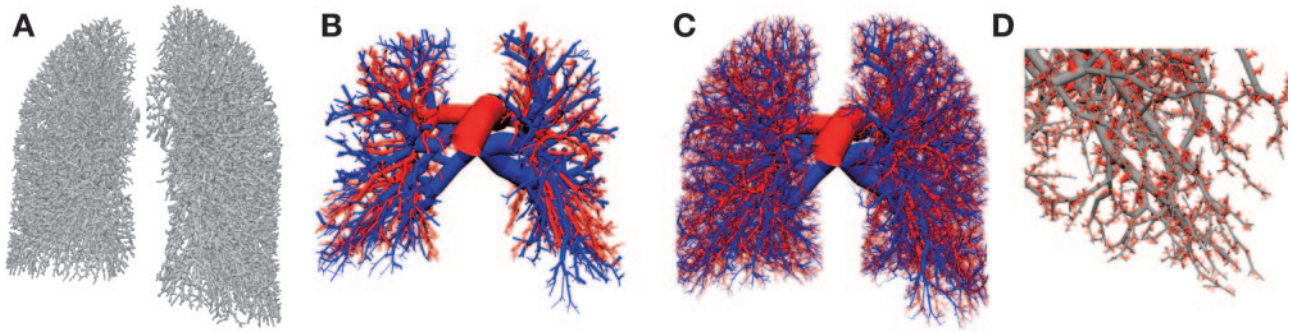

Fig. 4. *A*: rendered iso-surfaces of vessels segmented from multidetector row computed tomography (MDCT) data from the Lung Atlas. *B*: MDCT-derived arterial (red) and venous (blue) vessels. *C*: plus vessels generated into the lobar volume using the volume-filling branch (VFB) algorithm. *D*: close-in view of supernumerary vessels (red) with accompanying vessels (gray).

branches and diameter distribution as the anatomically based model, for comparison. The solution procedure is only applied to the left lung arterial geometry; the vast size of the full arterial model, including supernumerary vessels, creates a mathematical problem with very large memory requirements.

RESULTS

Approximately 2,500 branches in each of the arterial and venous trees were manually differentiated from the 1D skeleton of the arterial and venous trees derived from volumetric MDCT images. Arterial paths were identified to be between *generations 6* and *26* (mean 18), and venous paths were identified to be between *generations 6* and *23* (mean 15). The isolated MDCT-based vessels had equivalent to seven (incomplete) Strahler orders in the arterial tree and six (incomplete) Strahler orders in the venous tree (note that the venous tree has two less bifurcations at the heart inlet). Figure 4*A* shows the rendered iso-surfaces for the segmented blood vessels (both arterial and venous) from MDCT images, and Fig. 4*B* shows the vessels derived from MDCT data.

Generation of accompanying vessels to the level of the respiratory bronchioles produced nearly 60,000 additional branches in each tree. The MDCT plus accompanying vessel arterial tree had a total of 11 Strahler orders, compared with 9 Strahler orders for the venous tree. Figure 4*C* shows the MDCT-based and accompanying vessel models for the arterial (red) and venous (blue) models. R_b for the arterial tree was 2.78 and for the venous tree was 2.93 (Table 1).

Addition of the supernumerary vessels increased the total number of vessel segments in the arterial model to ~375,000 and the total number in the venous tree to ~497,000. A close-in view of the supernumerary and accompanying vessels is shown in Fig. 4*D*. The complete model comprised a total of 12 arterial Strahler orders and 10 venous Strahler orders; that is, addition of the supernumerary vessels increased each tree by only one Strahler order. The Strahler R_b increased from 2.8 to 3.0 for the arterial tree and from 2.9 to 3.4 for the venous tree (Table 1), which is much closer to the anatomical values than the MDCT-based plus accompanying vessel models.

Branching angles calculated for the full vessel model, for the conducting airway model from Tawhai et al. (29), and from anatomical studies of the airway tree are listed in Table 2. Branching angles (θ_{branch} and γ) for the accompanying arterial and venous trees are very similar to those for the conducting airway network. The addition of supernumerary vessels increases θ_{minor} and decreases θ_{major}.

Figure 5 plots Strahler order against number of branches for the model at all three stages of development (MDCT, plus accompanying vessels, plus supernumerary vessels) and compares with estimated numbers of branches from anatomical studies (13, 15).

The Poiseuille flow solution in the arterial model of the left lung is plotted with respect to the Strahler branch order number, with and without supernumerary vessels, in Fig. 6. The Poiseuille flow solution within a symmetric model is

Table 1. *Strahler-based branching, diameter, and length ratios for three stages of model development: MDCT vessels, plus VFB vessels, plus supernumerary vessels, compared with anatomical data*

	MDCT Vessels		+VFB Vessels		+Supernumerary Vessels		
	Ratio	R^2	Ratio	R^2	Ratio	R^2	Anatomical Data
R_b arteries	1.29	0.16	2.78	0.99	3.04	1.00	3.03 (6–17) (Ref. 13), 3.36 (1–15) (Ref. 17)
R_d arteries	1.57	1.00	1.57	1.00	1.57	1.00	1.60 (1–17) (Ref. 13), 1.56 (1–15) (Ref. 17)
R_l arteries	1.42	0.77	1.52	0.92	1.50	0.95	1.49 (1–14) (Ref. 13), 1.49 (1–15) (Ref. 17)
R_b veins	1.82	0.94	2.93	0.99	3.41	1.00	3.30 (1–17) (Ref. 15), 3.33 (1–15) (Ref. 17)
R_d veins	1.70	1.00	1.65	0.99	1.66	1.00	1.69 (7–14) (Ref. 15), 1.58 (1–15) (Ref. 17)
R_l veins	1.83	0.98	1.65	0.89	1.64	0.94	1.68 (7–14) (Ref. 15), 1.50 (1–15) (Ref. 17)

MDCT, multidetector row computed tomography; VFB, volume-filling branch; R_b, branching ratio; R_d, diameter ratio; R_l, length ratio. The numbers in parentheses in the anatomical data list represent the Strahler order number range for which the ratio was determined. The data from Ref. 17 used the diameter-defined Strahler ordering method; therefore, the main comparative data considered are that of Refs. 13 and 15, which are based on the Strahler ordering system.

Table 2. *Branching angles of the model generated using a combination of MDCT-derived vessels, VFB algorithm, and supernumerary vessel algorithm, compared with model and anatomical data for the conducting airways*

	Full Arterial Model	Full Venous Model	MDCT + VFB Arteries	MDCT + VFB Veins	Airway Model (29)	Published Airway Data
θ_{branch}	47.29±42.88	51.52±42.50	49.37±29.04	50.79±29.39	50.31±28.92	37.28 (14); 39, 43 (25)
γ	83.27±55.58	81.93±53.52	89.24±45.86	89.91±44.60	89.99±43.28	79 (25); 90 (12)
θ_{minor}	83.25±19.71	83.19±18.68	53.32±29.45	54.35±29.57	53.00±20.02	
θ_{major}	11.32±26.50	19.85±35.46	45.41±28.08	47.23±28.77	47.63±28.56	

Values are means ± SD in degrees. θ_{branch}, angle between parent and child branch; γ, rotation angle; θ_{minor}, angle between parent and minor child branch; θ_{major}, angle between parent and major child branch. Values from anatomical studies in the last column are followed by their reference numbers in parentheses.

also included for comparison. While this is only a very simplistic flow solution, the results demonstrate that, with increasing vascular asymmetry, especially with the addition of supernumerary vessels, the flow distribution becomes increasingly heterogeneous, displaying the importance of an anatomically accurate geometric model for the use in functional simulations.

DISCUSSION

Studies into the origin of blood flow heterogeneity in the lung have highlighted the prominent functional significance of the asymmetric branching structure of the pulmonary vasculature, suggesting that gravitational factors are a minor determinant of flow distribution (7). Previous studies have highlighted the intimate relationship between structure and function in the pulmonary circulatory system through both computational (3, 19, 24) and experimental investigations (7, 8). The development of a computational model of normal human pulmonary vascular structure can be applied to understanding normal hemodynamics and investigating the functional changes occurring in pulmonary vascular diseases as a result of vascular remodeling. The present study has developed an anatomically based finite element model of the human pulmonary macrocirculation that is suitable for application in such studies. The largest arterial and venous vessels were identified from MDCT scans from the Lung Atlas (20). This technique enables a more accurate description of vessel geometry and allows patient- and species-specific models to be generated. A volume-filling algorithm (31) was initiated from the MDCT-derived vessel endpoints to create a mathematical representation of the smaller accompanying blood vessels unidentifiable from MDCT images. The algorithm "grows" these vessels into an MDCT-defined pleural host volume down to the equivalent level of the respiratory bronchioles. This creates arterial and venous trees, which are somewhat governed by the shape of the lobe surfaces and the positions of the initial MDCT-derived vessels, thereby producing a more realistic, integrated model.

Tawhai et al. (29) investigated the influence of lobar geometry and the effect of using MDCT-derived vessels as starting points, as opposed to lobar branches when using the VFB algorithm on the R_b of the conducting airway model. The VFB algorithm was generated into the left and right lung volumes,

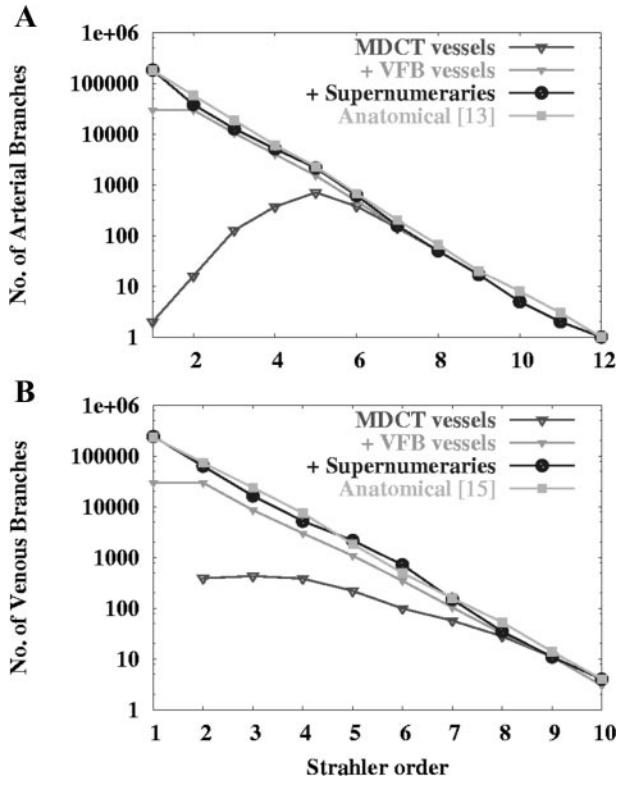

Fig. 5. Strahler order number vs. number of branches showing the progression of the model toward anatomical data for the arterial (*A*) and the venous (*B*) network. Plots show the number of branches from MDCT data, plus VFB vessels, and plus supernumerary vessels.

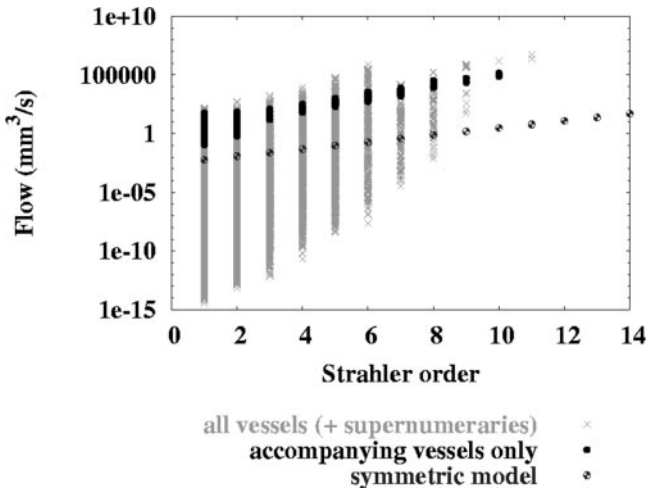

Fig. 6. Simple Poiseuille flow solutions (mm^3/s) in the arterial network of the left lung plotted with respect to the Strahler branch order number: results displayed with and without supernumerary vessels. The Poiseuille flow solution within a symmetric model (consisting of 14 Strahler orders, left lung only for consistency) is also included to highlight the significant effect of vascular geometry on flow results.

as opposed to the five separately defined lobes; this caused the Strahler-based R_b to decrease by 7.5%, demonstrating that the lobar constraining surfaces contribute to the asymmetry of the pulmonary trees. Generation of the VFB vessels from lobar branches decreased the R_b a further 5.3% from the initial R_b, indicating that the more accurate definition of large vessels via MDCT also increased the asymmetry of the tree. Tawhai et al. show that the branching geometry of the airway tree (and hence the geometry of the accompanying vessels) is modeled well by the VFB algorithm, regardless of the initial number of MDCT vessels. These comparisons were not sought to be reproduced in this study; however, similar behavior has been observed in the current vascular model. This may have implications for generating vascular models for different species, where the shape of the lung is significantly more asymmetric than the human lung.

The MDCT imaging used contrast agent injected into the pulmonary circulation to enhance the contrast between the blood vessels and surrounding tissue. This, however, resulted in an augmented arterial-venous data set, from which it was very difficult to extract the separate trees. The segmented images, shown in Fig. 4*A*, contain both the arterial and venous vessels. There were several points where the two trees met and appeared to join. The two trees were separated by visually predicting which vessels belonged to which system; therefore, some uncertainty remains over whether each of the vessels distinguished is correctly allocated to the arterial or venous system. The algorithm used to generate the centerline data in this study resulted in centerlines that were not always accurately located. The complex, intertwining nature of the pulmonary vasculature meant that several of the centerlines went outside of the vessel boundaries and crossed over to meet adjacent vessels. The centerline algorithm also superimposed several bifurcation points on top of each other, so it appeared as if there were multiple branches emerging from a single branch point. In reality, it is most likely that the system forms only bifurcations in close succession, and possibly trifurcations, but not higher orders than this; corrections were made to reflect this and ensure that no vessels overlapped. On inspection of the actual MDCT-segmented vessel surfaces, it was apparent that most junctions were bifurcations, and for these reasons the vessels were selected manually. Diameter values for the larger vessels were not able to be derived via MDCT due to the same issues explained above, as the amount of uncertainty was too high. Segmentation algorithms and reconstruction techniques are constantly being improved, and, in the near future, it should be possible to use automated techniques to obtain more extensive MDCT-derived, patient-specific models of the arterial and venous trees (27). MDCT imaging enables the pulmonary vessels to be located and measured in vivo, thereby avoiding any vessel deformation that may occur during casting. The use of high-resolution imaging data also provides greater scope for establishing normative ranges of variation in geometry and vessel distention in different orientations or at different blood pressures, which is the goal of the Lung Atlas (20).

The present model allocates diameters based on the Strahler order number of each branch. For future functional investigations, the diameter relationships may be applied differently to achieve the desired tree qualities. As image processing technologies advance, it will be possible to obtain diameter values of the largest vessels via MDCT images, providing a much more accurate model by enabling in vivo data to be used directly as opposed to information derived from casts. Pulmonary arterial diameters have previously been obtained via computed tomography (CT) (18, 21, 35), but relatively few vessels were measured in these studies.

Figure 5 clearly shows that the vessel set extracted via MDCT was not complete. Anatomical measures have shown that there is a linear relationship between the Strahler order number and the log of the number of branches in each order. For example, it appears that the vessel set is complete in the arterial network from *orders 7–12*, and for the venous tree only from Strahler *orders 8–10*. After these points, the line in the semilogarithmic plot of Strahler order vs. branch number delineates from the expected straight line.

Each airway is known to have an accompanying artery and vein, but, in addition to these vessels, there are also many extra blood vessels unaccompanied by airways: the "supernumerary" vessels (5). Morphological studies have shown that pulmonary vascular branching is not a classical dichotomy and that the supernumerary vessels are a characteristic feature of pulmonary arterial and venous trees (4, 5). Supernumerary vessels are not found on angiograms, due to lack of filling, because of the 90° angle they make to the axial branch (5) and the presence of a sphincter, which has been found at the entrance of bovine supernumerary vessels (26). It is thought that these vessels provide a reserve volume during increased cardiac output, such as during exercise (26). Also, in the adult, it is these vessels that can provide collateral blood flow if the conventional vessels are occluded (4). The limited known characteristics of the supernumerary vessels were exploited to develop a computational algorithm to incorporate these vessels into the model. The development of this algorithm was based on the small amount of available anatomical data. The representation of these vessels is, therefore, very dependent on the accuracy of measurements from casts. It is very likely that many of these vessels were not adequately perfused during the casting procedure or that some of these vessels may have been removed in the trimming routine. It can be seen in Fig. 5 that the addition of the supernumerary vessels increases the number of branches in the last few Strahler orders of the model, bringing the branch number per Strahler order close to the anatomical data. This algorithm may be easily adapted in the future, by modifying the R_d of accompanying to supernumerary vessel, frequency of supernumerary vessels to accompanying vessels, or by modifying the R_l to R_d, as more measured data become available. The frequency values determined to produce the most accurate model, 2.5:1 for the arteries and 3:1 for the veins, are relatively close to the predicted ratios of accompanying to supernumerary vessels of 2.8:1 and 3.5:1 for the arteries and veins, respectively.

The Strahler-based R_b, shown in Table 1, are compared with ratios calculated from anatomical data. Only the Strahler ratios are calculated, not Horsfield-based ratios, because the Strahler ordering system better describes the asymmetric blood vessel geometry. The R_b increase from relatively low values at the MDCT vessel start point to values very close to the anatomical values for the complete model. The model R_d and R_l are all within 2.5% of the anatomical values. The asymmetry of the full model arterial and venous trees is, therefore, closely

representative of the measured asymmetry of the human pulmonary vascular trees.

The full model branch angles (Table 2) are compared with published values from the conducting airway model developed by Tawhai et al. (29) and anatomical values for the conducting airways. The branch angle in the MDCT plus accompanying vessel model is higher than the published airway branch angles due to increasing branching angles toward the tree periphery, as explained in Ref. 29. Addition of supernumerary vessels increases the minor branch angle and decreases the major branch angle with respect to the MDCT plus accompanying vessel model, by ~30° for each angle, and for each of the arterial and venous models. This large change in major and minor branch angle reflects the difference in branching geometry of the supernumerary vessels. That is, the minor branch angle in the full model is heavily weighted by supernumerary branching angles close to 90°, and the major branch angle now includes "zero" branch angles comprising the continuation of the parent vessel.

A very simple flow solution has been implemented within the arterial model geometry (of the left lung only) with and without supernumerary vessels to investigate the influence of the vascular branching structure on flow heterogeneity. The model results (with and without supernumeraries) are also compared with Poiseuille flow results within a symmetric model. This highlights the influence of the vascular branching geometry on flow heterogeneity. Symmetric model flow results are homogeneous with respect to Strahler branch order. Flow heterogeneity in the anatomically based model (excluding supernumerary vessels) is increased. Addition of the supernumerary vessels further increases this heterogeneity. These flow results demonstrate the potential of the model, but they are not very realistic, mainly because the vessels are treated as rigid tubes. Sphincters have been identified at the entrance to supernumerary vessels in bovine lungs (26), and this factor is also not accounted for in the present model. Without developing a more sophisticated model to simulate flow in the supernumeraries, it is difficult to clearly display the effect they have on perfusion. In reality, it is most likely that supernumerary vessel perfusion is minimal. More realistic solutions will be obtained when a complete flow circuit is achieved by coupling the arterial and venous geometries via a model of the microcirculation.

This model has been developed to represent the complex geometry found in the pulmonary circulatory system, for application in future, more detailed structure-functional investigations. The present study is concerned with presenting only the geometric model (and a preliminary Poiseuille flow solution). The authors did not want to "overreach" by proposing how the model would or could be used for functional simulations. The methods for coupling structure and function are well established: the model is simply a finite element mesh within which a system of mathematical equations can be solved, as has previously been demonstrated for blood flow through the pulmonary capillary (2) and coronary vessels (28). The derivation of lobar and large-vessel geometry from MDCT enables the creation of subject-specific, anatomically based models of the pulmonary system with relatively low effort. As imaging and image processing techniques improve, it will be possible to derive an increasing amount of information from imaging modalities such as CT. The increasing spatial and temporal resolution of CT imaging will enable unification of structure-to-function correlations via imaging and computational techniques. This amalgamation provides potential applications in tracking structural changes via imaging (remodeling, vasoconstriction) and investigating the consequences on global lung function via modeling. This is the first known attempt to explicitly incorporate the supernumerary vessels into a vascular model; it is hoped that the development of this model will aid in future computational investigations to determine the functional significance and behavior of these vessels.

ACKNOWLEDGMENTS

The authors thank Drs. Eric Hoffman, Geoff McLennan, Juerg Tschirren, Joe Reinhardt, and Hidenori Shikata from the University of Iowa for providing the MDCT segmented images and tree skeletonization.

GRANTS

This work was supported by a doctoral fellowship provided by the Foundation for Research, Science and Technology New Zealand (FRST), and RSNZ Marsden Grant UOA-01–070.

REFERENCES

1. **Bennett SH, Goetzman BW, Milstein JM, and Pannu JS.** Role of arterial design on pulse wave reflection in a fractal pulmonary network. *J Appl Physiol* 80: 1033–1056, 1996.
2. **Burrowes K, Tawhai M, and Hunter PJ.** Modeling RBC and neutrophil distribution through an anatomically based pulmonary capillary network. *Ann Biomed Eng* 32: 585–595, 2004.
3. **Dawson CA, Krenz GS, Karau KL, Haworth ST, Hanger CC, and Linehan JH.** Structure-function relationships in the pulmonary arterial tree. *J Appl Physiol* 86: 569–583, 1999.
4. **deMello D and Reid LM.** Arteries and veins. In: *The Lung: Scientific Foundations*, edited by Crystal RG and West JB. New York: Raven, 1991.
5. **Elliot FM and Reid L.** Some new facts about the pulmonary artery and its branching pattern. *Clin Radiol* 16: 193–198, 1965.
6. **Fernandez J, Mithraratne P, Thrupp S, Tawhai MH, and Hunter PJ.** Anatomically based geometric modelling of the musculo-skeletal system and other organs. *Biomech Model Mechanobiol* 2: 139–155, 2004.
7. **Glenny RW, Bernard S, Robertson HT, and Hlastala MP.** Gravity is an important but secondary determinant of regional pulmonary blood flow in upright primates. *J Appl Physiol* 86: 623–632, 1999.
8. **Glenny RW, Polissar L, and Robertson HT.** Relative contribution of gravity to pulmonary perfusion heterogeneity. *J Appl Physiol* 71: 2449–2452, 1991.
9. **Glenny RW and Robertson HT.** Fractal modeling of pulmonary blood flow heterogeneity. *J Appl Physiol* 70: 1024–1030, 1991.
10. **Haefeli-Bleuer B and Weibel ER.** Morphometry of the human pulmonary acinus. *Anat Rec* 220: 401–414, 1988.
11. **Hlastala MP and Glenny RW.** Vascular structure determines pulmonary blood flow distribution. *News Physiol Sci* 14: 182–186, 1999.
12. **Horsfield K.** Anatomical factors influencing gas mixing and distribution. In: *Gas Mixing and Distribution in the Lung*, edited by Engel LA and Paiva M. New York: Dekker, 1985.
13. **Horsfield K.** Morphometry of the small pulmonary arteries in man. *Circ Res* 42: 593–537, 1978.
14. **Horsfield K and Cumming G.** Angles of branching and diameters of branches in the human bronchial tree. *Bull Math Biophys* 29: 245–259, 1967.
15. **Horsfield K and Gordon WI.** Morphometry of pulmonary veins in man. *Lung* 159: 211–218, 1981.
16. **Horsfield K and Woldenberg MJ.** Diameters and cross-sectional areas of branches in the human pulmonary arterial tree. *Anat Rec* 223: 245–251, 1989.
17. **Huang W, Yen RT, McLaurine M, and Bledsoe G.** Morphometry of the human pulmonary vasculature. *J Appl Physiol* 81: 2123–2133, 1996.
18. **Karau KL, Johnson RH, Molthen RC, Dhyani AH, Haworth ST, Hanger CC, Roerig DL, and Dawson CA.** Microfocal X-ray CT imaging and pulmonary arterial distensibility in excised rat lungs. *Am J Physiol Heart Circ Physiol* 281: H1447–H1457, 2001.

19. **Krenz GS, Linehan JH, and Dawson CA.** A fractal continuum model of the pulmonary arterial tree. *J Appl Physiol* 72: 2225–2237, 1992.
20. **Li B, Christensen GE, Hoffman EA, McLennan G, and Reinhardt JM.** Establishing a normative atlas of the human lung: intersubject warping and registration of volumetric CT images. *Acad Radiol* 10: 255–265, 2003.
21. **Liu YH, Hoffman EA, and Ritman EL.** Measurement of three-dimensional anatomy and function of pulmonary arteries with high speed x-ray computed tomography. *Invest Radiol* 22: 28–36, 1987.
22. **Maina JN and Gils PV.** Morphometric characterization of the airway and vascular systems of the lung of the domestic pig *Sus scrofa*: comparison of the airway, arterial and venous system. *Comp Biochem Physiol A* 130: 781–798, 2001.
23. **Palagyi K, Sorantin E, Balogh E, Kuba A, Halmai C, Erdohelyi B, and Hausegger K.** A sequential 3D thinning algorithm and its medical applications. In: *Proceedings of Information Processing in Medical Imaging: 17th International Conference, IMPI 2001, Davis, CA, USA, June 18–22, 2001*. Berlin: Springer Verlag, 2001, p. 409–415.
24. **Parker JC, Cave CB, Ardell JL, Hamm CR, and Williams SG.** Vascular tree structure affects lung blood flow heterogeneity simulated in three dimensions. *J Appl Physiol* 83: 1370–1382, 1997.
25. **Sauret V, Halson PM, Brown IW, Fleming JS, and Bailey AG.** Study of the three-dimensional geometry of the central conducting airways in man using computed tomographic (CT) images. *J Anat* 200: 123–134, 2000.
26. **Shaw AM, Bunton DC, Fisher A, McGrath JC, Montgomery I, Daly C, and MacDonald A.** V-shaped cushion at the origin of bovine pulmonary supernumerary arteries: structure and putative function. *J Appl Physiol* 87: 2348–2356, 1999.
27. **Shikata H, Sonka M, and Hoffman EA.** Fully automated pulmonary vascular tree segmentation using human and sheep 3D CT data. In: *Proceedings of the American Thoracic Society, 100th International Conference, May 21–26, 2004, Orlando, FL. Orlando, FL*: Am. Thoracic Soc., 2004.
28. **Smith NP, Pullan AJ, and Hunter PJ.** An anatomically based model of transient coronary blood flow in the heart. *SIAM J Appl Math* 62: 990–1018, 2002.
29. **Tawhai M, Hunter PJ, Tschirren J, Reinhardt J, McLennan G, and Hoffman EA.** CT-based geometry analysis and finite element models of the human and ovine bronchial tree. *J Appl Physiol* 97: 2310–2321, 2004.
31. **Tawhai M, Pullan AJ, and Hunter PJ.** Generation of an anatomically based model of the conducting airways. *Ann Biomed Eng* 28: 793–802, 2000.
32. **Weibel ER.** *Morphometry of the Human Lung*. Berlin: Springer-Verlag, 1963.
33. **Weibel ER.** *The Pathway for Oxygen: Structure and Function in the Mammalian Respiratory System.* Cambridge, MA: Harvard University Press, 1984.
34. **West JB, Dollery CT, and Naimark A.** Distribution of blood flow in isolated lung; relation to vascular and alveolar pressures. *J Appl Physiol* 19: 713–724, 1964.
35. **Wood S, Zerhouni E, Hoford J, Hoffman EA, and Mitzner W.** Measurement of three-dimensional lung tree structures by using computed tomography. *J Appl Physiol* 79: 1687–1697, 1995.